NJC

Accepted Manuscript

This is an *Accepted Manuscript*, which has been through the Royal Society of Chemistry peer review process and has been accepted for publication.

Accepted Manuscripts are published online shortly after acceptance, before technical editing, formatting and proof reading. Using this free service, authors can make their results available to the community, in citable form, before we publish the edited article. We will replace this *Accepted Manuscript* with the edited and formatted *Advance Article* as soon as it is available.

You can find more information about *Accepted Manuscripts* in the Information for Authors.

Please note that technical editing may introduce minor changes to the text and/or graphics, which may alter content. The journal's standard Terms & Conditions and the Ethical guidelines still apply. In no event shall the Royal Society of Chemistry be held responsible for any errors or omissions in this *Accepted Manuscript* or any consequences arising from the use of any information it contains.

ROYAL SOCIETY OF CHEMISTRY

www.rsc.org/njc

Journal Name

ARTICLE

Insights into the Pore Structure of KIT-6 and SBA-15 Ordered Mesoporous Silica – Recent Advances by Combining Physical Adsorption with Mercury Porosimetry

/Received 00th January 20xx,
Accepted 00th January 20xx

DOI: 10.1039/x0xx00000x

www.rsc.org/

Rémy Guillet-Nicolas,[a] Riaz Ahmad,[a] Katie A. Cychosz,[a] Freddy Kleitz,[b*] and Matthias Thommes[a*]

We have performed a systematic study of N_2 adsorption at 77 K and Hg porosimetry at 298 K experiments on highly ordered KIT-6 and SBA-15 silicas exhibiting noticeably different pore structures with pore diameters in the 7-11 nm range. Accurate pore structure analysis was performed by applying proper NLDFT methods to the N_2 physisorption data. Mercury intrusion/extrusion experiments on KIT-6 silicas (up to 415000 kPa) showed quite remarkably no collapse of the pore structure. To the best of our knowledge, this is the first successful example of Hg porosimetry on KIT-6 materials. Hence, it was possible to utilize KIT-6 mesoporous molecular sieves for quantitatively testing the validity of the Washburn equation applied to mercury intrusion for pore size analysis. KIT-6 silicas also allowed for investigating the analogies between condensation-evaporation mechanisms of wetting (N_2 at 77 K) and non-wetting fluids (Hg at 298 K) as a function of pore size confirming the thermodynamic consistency between Hg intrusion/extrusion and capillary evaporation/condensation. Contrary to KIT-6 silicas, Hg porosimetry experiments on SBA-15 materials of idential pore diameter show inconsistent behavior in a sense that both reversible Hg intrusion/extrusion data and partical collapse of the pore structure were observed. Our work clearly demonstrates that combining advanced physical adsorption and Hg porosimetry studies provide a more thorough understanding of textural features and shed some light into fundamental questions concerning the effect of confinement on the phase behavior of wetting and non-wetting fluids.

Introduction

In recent years, significant advancement has been made in the experimental characterization of porous materials.[1,2,3,4] Major progress has been achieved with regard to the understanding of adsorption phenomena in narrow pores (for reviews see refs 5 and 6), which has led to significant improvements in the pore size characterization. This progress was supported by a number of developments: (i) the discovery of novel highly ordered mesoporous (e.g., MCM-41, MCM-48) and micro-mesoporous model materials (e.g., SBA-15), which exhibit a uniform pore structure and morphology and can therefore be used as model adsorbents to test theories of gas adsorption; (ii) carefully performed adsorption experiments; (iii) the application of methods, such as the Non-Local Density Functional Theory (NLDFT) and computer simulation methods (e.g., Monte-Carlo and Molecular-Dynamic simulations). These methods are based on statistical mechanics and allow describing the configuration of the adsorbed phase in pores on a molecular level, in contrast to classical methods, which are based on macroscopic thermodynamic assumptions (e.g., methods based on the Kelvin approach such as BJH) and tend to significantly underestimate the pore size of narrow mesopores, i.e., up to 25-30 % for pore widths below 10 nm.[4,6, 7] Pore size analysis data for microporous and mesoporous molecular sieves obtained with these novel methods agree very well with the results obtained from independent methods (based on XRD, TEM, etc.), and allow characterizing a sample over the complete micropore/mesopore size range. Appropriate methods for pore size analysis based on NLDFT and molecular simulation are meanwhile commercially available for many adsorptive/adsorbent systems. These recent advances in physical adsorption characterization are summarized in the 2015 IUPAC recommendations.[8]

While physisorption allows assessing pore sizes from the micropore range (pore widths < 2 nm) and mesopore range (pores widths between 2-50 nm), the generally accepted and widely employed method for textural analysis of macroporous materials (pore widths > 50 nm) is mercury porosimetry. The main attraction of the latter technique is that it allows pore

[a] *Quantachrome Instruments, 1900 Corporate Drive, Boynton Beach, FL, 33426, USA. E-mail: Matthias.thommes@quantachrome.com*
[b] *Department of Chemistry and CERMA, Université Laval, Québec, QC, G1V0A6, Canada. E-mail: freddy.kleitz@chm.ulaval.ca*

Electronic Supplementary Information (ESI) available: Pore size analysis of KIT-6A, KIT-6B, SBA-15IC and SBA-15PC, low angle XRD patterns of KIT-6 materials and comparison of isotherm of a wetting fluid and corresponding equivalent gas sorption isotherm of a non-wetting fluid for KIT-6A and KIT-6B. See DOI: 10.1039/x0xx00000x

size analysis to be undertaken over a wide range of mesopore-macropore widths (routinely, from ca. 0.04 μm to ca. 400 μm) in a fast and highly reproducible way. In addition, mercury intrusion/extrusion data contain information regarding the surface area, particle size distribution, tortuosity, permeability, and compressibility of porous materials. Furthermore, the technique can provide useful information relating to the pore shape, pore network effects and density (skeletal and bulk density).[5,6,9,10]

However, in contrast to physical adsorption of fluids such as nitrogen and argon at their boiling temperatures (i.e., 77 K and 87 K, respectively), where the adsorbed phase completely wets the pore walls, mercury (at room temperature) does not wet the majority of materials and therefore (hydrostatic) pressure P_h must be applied to force mercury into the pores. The relationship between the applied pressure P_h and the pore radius r is given by the Washburn equation:[11]

$$P_h r = -2\gamma \cos\theta \quad (1.1)$$

where γ is the surface tension of mercury, and θ is the contact angle between the mercury and the solid pore (contact angles of mercury with various solids can be found for instance in ref. 1, 9 and 12).

A significant feature of mercury porosimetry curves is the occurrence of hysteresis between the intrusion and extrusion branch. In addition, entrapment is often observed, i.e., mercury remains contained in the porous network after extrusion. It has long been recognized[13,14,15,16,17,18] that an understanding of the hysteresis and entrapment phenomena is most important in order to be able to obtain an meaningful pore size analysis[19,20,21,22,23,24,25,26,27,] and different mechanisms have been proposed to explain intrusion/extrusion hysteresis. It is now well understood, that thermodynamically, the mercury intrusion and the capillary evaporation follow similar pathways. [28 , 29 , 30 , 31] In fact, the shape of a mercury intrusion/extrusion hysteresis loop often agrees quite well with that of the corresponding gas adsorption loop caused by capillary evaporation/condensation. Hence, the underlying mechanisms for hysteresis are analogue, i.e. similar to pore condensation hysteresis in gas adsorption, mercury intrusion/extrusion hysteresis is caused by nucleation barriers associated with the formation of a vapor-liquid interface during extrusion (which corresponds to the adsorption in gas adsorption). Mercury intrusion/extrusion hysteresis has also been discussed in the past within the context of contact angle hysteresis, assuming differences in advancing and receding contact angles.[23,24] In addition network models take into account that pore blocking or percolation affects the pressure where mercury intrudes the pore system (analog to the evaporation/desorption of nitrogen from pore networks).[23,25] Hence, in this case the pore size obtained from the intrusion branch reflects the pore entrance/pore neck diameter. By applying complex network models based on percolation theory, limited amount of structural information can be obtained from the intrusion/extrusion hysteresis loop.[25] Scanning the hysteresis loop in combination with the application of advanced network models can also provide information about the pore network and the solid structure.[18]

As mentioned above, often entrapment is observed, i.e., mercury remains contained in the porous network. The entrapment phenomenon is believed to be associated with kinetic effects during mercury extrusion, coupled with the tortuosity of disordered pore network and the surface chemistry of the material.[19,22] Recent systematic intrusion/extrusion experiments on materials with well-defined pore systems[17] and molecular simulation studies[28-30] indicated that entrapment is associated with the rupture of mercury bridges in pore constrictions during extrusion leading to entrapment in ink-bottle pores. This is in agreement with recent studies involving Grand Canonical Monte Carlo simulations using both Glauber dynamics and Kawasaki dynamics[28-30], which suggest that mercury entrapment is caused by a decrease in the rate of mass transfer associated with the fragmentation of liquid during extrusion. This leads to a configuration whereby droplets of mercury are surrounded by a vapor phase. The fragmentation slows down the rate of mass transfer of fluid from the porous material. It reflects a mechanism of evaporation of liquid from the entrapped droplets and diffusion of this vapor to the external surface. As a consequence, it has been observed that (given equilibration characteristics) samples with small pores, low porosity and highly tortuous nature exhibit larger amounts of entrapment as compared to samples with large pores and high porosity.[28]

Previous mercury intrusion/extrusion experiments into hierarchically structured model meso/macroporous silica monoliths indeed revealed mercury intrusion/extrusion into the mesopores without any appreciable amount of entrapment.[34] This serves as an indication that the rate of mass transfer in and out of the mesopores appears to be fast enough to avoid fragmentation of liquid during extrusion (which would lead to entrapment). The reason for the lack of entrapment could be correlated with the unique texture of these hierarchical pore networks consisting of a well-defined mesopore systems surrounded by macroporous through-pores.[31] However, the vast majority of mercury porosimetry experiments reported in the literature had been thus far performed on disordered porous materials, while the progress and validation of gas adsorption methods was based on experiments utilizing mesoporous molecular sieves, such as MCM-41, SBA-15. Unfortunately, due to their limited mechanical stability, these ordered mesoporous materials have, in contrary to gas adsorption, not been widely used as model materials for improving the understanding of the mercury intrusion/extrusion mechanism and therefore used for the validation of mercury porosimetry (e.g., 19,30,31, 32 , 33 , 34 , 35 , 36 , 37). Recent experimental work focusing on mercury intrusion/extrusion into MCM-41 and SBA-15 silicas exhibiting pseudo 1D pore structure again pointed out this problem,[36] with the consequence that the interpretation of the obtained intrusion/extrusion data was not straightforward.

Within this framework, we focus in this contribution on the systematic experimental study of mercury intrusion/extrusion

into mesoporous molecular sieves of 3D pore structure, i.e., KIT-6 silicas, and compare the obtained intrusion/extrusion behavior with mercury porosimetry experiments obtained on SBA-15 samples. KIT-6 and SBA-15 silicas can be seen as the large-pore analogues of the MCM-48 and MCM-41 solids, respectively.[38,39,40] In terms of pore structure, the mesopore system of the cubic KIT-6 silica exhibits a highly interconnected network which is based on two continuous interpenetrating sub-networks of channels separated by an amorphous silica wall.[41,42] The mesopore system of SBA-15 is composed of a hexagonal arrangement of cylindrical-like pores surrounded by amorphous silica walls. Both materials can exhibit, a secondary pore system in their framework walls (i.e., intra-wall pores).[41,43,44,45,46,47,48] These intra-wall pores are usually in the micropore/small mesopores range and are highly dependent on the details of the synthesis. Modulation of this complementary porosity allows to finely tune the porous topology of the materials.[43,46,49] This adjustable porosity is a key feature of these large pore ordered mesoporous silicas and is of tremendous importance for many applications (e.g., in catalysis[50,51] adsorbents/separation,[52,53] drug delivery,[54] and starting mold for nanocasting procedures[55,56,57]).

To our knowledge, we report the first systematic experimental study of mercury intrusion/extrusion using cubic *Ia*3*d* KIT-6 silicas with pore diameters ranging from ca. 7 nm up to 11 nm and compare the results obtained with data in SBA-15 silicas of similar pore sizes. Utilizing these mesoporous molecular sieves allows us also to investigate the analogies between condensation-evaporation mechanisms of a wetting fluid (N_2 at 77K) and of non-wetting fluid (Hg at room temperature) and discuss consequences for pore size analysis by mercury porosimetry.

Experimental

Chemicals

The Pluronic triblock copolymer (P123, $EO_{20}PO_{70}EO_{20}$, MW = 5800) and tetraethoxysilane (TEOS, 98 %) were purchased from Sigma-Aldrich. Hydrochloric acid (HCl, 37. 5%) was purchased from Fisher Scientific and. n-butanol (99.9 %) was purchased from Fluka. Chemicals were used as received, without further purification.

Materials

KIT-6 materials were synthesized following the procedure reported by Ryoo *et al.*[39] Typically, 7.9 g of P123 was dissolved in 287 g of distilled water and 14.6 g of HCl (37.5%) under vigorous stirring at 35 °C. After complete dissolution, 7.9 g of n-butanol (99.9%, Fluka) was added to the mixture and after one hour, 20.4 g of TEOS was added at once to the homogeneous solution. The resulting mixture was left under stirring at 35 °C for 24 hours. Thereafter the synthesis was put in an oven for hydrothermal treatment at 100 °C (KIT-6A) or 130 °C (KIT-6B) for another 24 h under static conditions. Silica products were then filtered hot and dried at 100 °C for 24 hours. For template removal, the as-synthesized silica powders were first shortly slurred in an ethanol-HCl mixture and were subsequently calcined at 550 °C for 5 h under air flow. In order to reach larger pore sizes, sulfuric acid treatment was also performed on as-synthesized KIT-6B, prior to calcination.[58] Briefly, 1.0 g of as-synthesized KIT-6B sample was mixed with 100 mL of 45 wt % H_2SO_4 solution and heated at 95 °C for 24 hours. After the reaction, the products were washed with water until the eluent became neutral, then washed with acetone, and dried overnight at 80 °C. Finally, to remove the occluded EO chains in the silica walls, the acid treated samples were further heated in air at 540 °C. The resulting sample is denoted KIT-6C.

SBA-15 materials were synthesized following the procedure reported by Choi *et al.*[59] SBA-15 samples were prepared under two different synthetic conditions in order to modulate the structure and porosity of the resulting materials. The molar composition of the starting reaction mixture was *x* TEOS/0.017 P123/1.47 HCl/97.6 H_2O, with *x* = 1 (SBA-15IC) or 1.33 (SBA-15PC). Typically, 8.0 g of P123 was dissolved in 146.25 g of distilled water and 4.46 g of HCl (37.5%) under vigorous stirring at 30 °C (SBA-15IC) or 35 °C (SBA-15PC). After complete dissolution, adequate quantity of TEOS was added at once to the homogeneous solution. The resulting mixture was left under stirring at the same temperature for 24 hours. Thereafter the synthesis was put in an oven for hydrothermal treatment at 90 °C (SBA-15IC) or 120 °C (SBA-15PC) for another 24 h under static conditions. Silica products were then filtered hot and dried at 100 °C for 24 hours. For template removal, the as-synthesized silica powders were first shortly slurred in an ethanol-HCl mixture and were subsequently calcined at 550 °C for 5 h under air flow.

Gas adsorption and mercury porosimetry experiments

Nitrogen adsorption–desorption isotherms were measured at liquid nitrogen temperature (77.4 K) using an Autosorb iQ automatic volumetric adsorption analyzer from Quantachrome (Boynton Beach, FL, USA). Prior to the measurements, the KIT-6 and SBA-15 samples were degassed at 200 °C for 8 hours under turbomolecular pump vacuum.

Mercury intrusion and extrusion experiments on KIT-6 and SBA-15 samples were performed at 25°C for wide range pressures ranging up to 415000 kPa by a Quantachrome Poremaster 60 instrument. Data acquisition was performed in the so-called continuous scanning mode, in which the rate of pressurization is controlled by the motor speed of the pressure generator system. The motor speed can be set to a fixed, constant value. However, it is also possible (with the help of a microcomputer) to adjust the pressurization and depressurization rate in inverse proportion to the rate of intrusion or extrusion respectively. Thus, the porosimeter provides maximum speed in the absence of intrusion or extrusion and maximum resolution and in most cases sufficient relaxation time (sampling time) when most required, i.e., when intrusion or extrusion is occurring rapidly with changing pressure. The use of this scanning mode allows obtaining high-resolution intrusion/extrusion curves. Surface tension of

mercury was assumed to be 484 mNm^{-1}. A contact angle of 145° was chosen, which has been found to be a reliable value, based on measurements performed on amorphous silica.[60,61]

Powder small angle XRD

Low-angle powder X-ray diffraction (XRD) patterns were recorded on a Rigaku Multiplex instrument operated at 2 kW, using Cu Kα radiation (KAIST, Daejeon, Republic of Korea). The XRD scanning was performed under ambient conditions in steps of 0.01°, with an accumulation time of 0.5 s.

Results and discussions

KIT-6 silicas materials were first characterized by gas physisorption at cryogenic temperature in order to access their porosity features. Nitrogen adsorption/desorption data obtained at 77.4 K for the different KIT-6 samples, presented in Figure 1a, evidenced the high structural order of the large pore cubic KIT-6 materials under investigation. As expected, all isotherms exhibit type IV with a H1 hysteresis loop. The steep capillary condensation and evaporation step observed for each isotherm is characteristic of high quality KIT-6 materials with narrow mesopore distribution. Moreover, the plateau-like region reached after the filling of the mesopores confirmed the negligible external surface area of the silicas making the Gurvitch rule a reliable way to calculate the total pore volume of each sample. The BET specific surface area values of the samples, obtained from the nitrogen adsorption data, i.e., 814 m^2/g, 559 m^2/g and 474 m^2/g for KIT-6A, KIT-6B and KIT-6C, respectively, are in good agreement with those reported previously for similar samples.[39,41,43,62]

Increasing the hydrothermal aging temperature results in materials (KIT-6A and KIT-6B) with substantially higher total adsorption capacity (and corresponding larger pore volumes, see table 1) which is also consistent with previous data.[39,41,49,62] Treating silica with sulfuric acid also results in an increase in the total pore volume (Table 1, KIT-6B and KIT-6C) being in line with previous results obtained for SBA-15 silicas.[58] Moreover, as shown in Figure 1b, the narrow pore size distribution of the samples was confirmed by the cumulative pore volume distributions obtained by applying the equilibrium model of non-local density functional theory (NLDFT method) on the desorption branches of nitrogen (77.4 K) isotherms considering cylindrical silica pores as a pore model. It is important to note that the assumption of cylindrical pore geometry for cubic *Ia3d* materials has already been discussed in recent studies and validated as a reasonable first approximation.[62,63,64] Furthermore, our advanced pore size analysis (Fig 1) confirms that both KIT-6B and KIT-6C do not exhibit any micropores nor narrow mesopores (< 5 nm), whereas a noticeable pore volume coming from narrower intra-wall meso- and micropores can be seen in the case of KIT6-A. These differences originate from the highly temperature-dependent behavior of the P123 copolymer, i.e., the aggregation and penetration of the EO chains inside the silica wall during the material synthesis.[43-48] The narrow pore size distribution of the large mesopores confirms the excellent homogeneity of the siliceous sieves. Note that the NLDFT methods implemented in this work have proven to provide (i) an accurate description of the experimental adsorption/desorption isotherms of fluids such as nitrogen (at 77.4 K) in siliceous materials with cylindrical pores, and (ii) accurate pore size distributions.[65,66] From the pore size distribution (PSD) curves, it is obvious that a simple variation of the hydrothermal aging temperature enables larger mesopore dimensions. Indeed, KIT-6A which was aged at 100 °C exhibits a main mesopore diameter of 8.5 nm whereas KIT-6B, which was aged at 130 °C exhibits pores of 9.4 nm (Figure 1c and Table 1). After acid treatment, the pore size of the KIT-6C sample was found to be 10.9 nm.

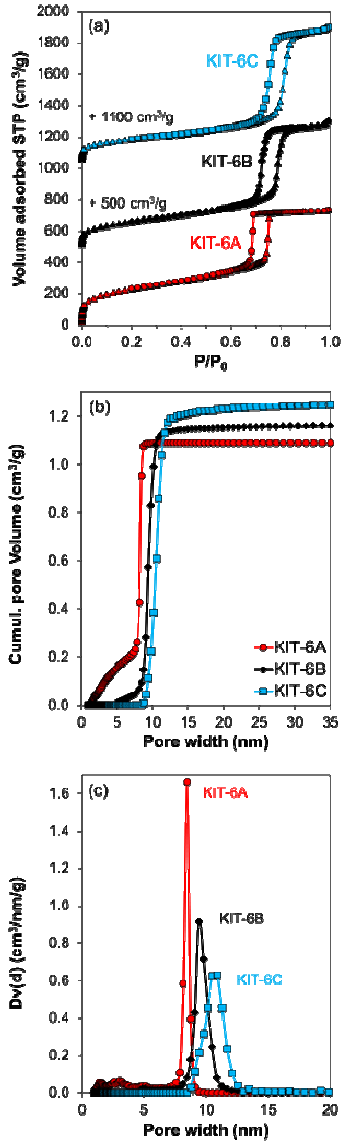

Fig. 1 N_2 at 77.4 K adsorption/desorption isotherms (a), corresponding NLDFT cumulative pore volumes (b) and pore size distributions (calculated from the desorption branches) (c) obtained for KIT-6 samples.

Table 1 Textural parameters of KIT-6 and SBA-15 samples derived from N2 physisorption isotherms and mercury porosimetry.

Sample	Mercury porosimetry		N_2 physisorption				
	Mesopore volume for $P_w \geq 4$ nm (cm^3/g)	Pore size (nm)	Total pore volume (cm^3/g)	NLDFT pore volume (cm^3/g)	BJH pore size (nm)	NLDFT pore size (nm)	BET (m^2/g)
KIT-6A	0.77	6.0	1.12	1.09	6.8	8.5	814
KIT-6B	0.83	7.1	1.18	1.16	7.7	9.4	559
KIT-6C	1.11	7.9	1.27	1.26	8.8	10.9	474
SBA-15C	0.55	5.4	0.84	0.82	6.0	7.6	674
SBA-15PC	0.35	5.1	0.96	0.91	6.0	7.6	661

The results of two consecutive intrusion/extrusion repeat cycles into the mesopores of the different KIT-6 samples (in linear scale) are shown in Figure 2a. After the first intrusion–extrusion cycle, some mercury remains entrapped in all three samples sample, so the hysteresis loop is not closing. However, in line with observations made for different model materials,[17,19,22,28-30] entrapment completely disappears in the second intrusion/extrusion cycle of each KIT-6 samples (Figure 2a, dash lines), confirming again that entrapment and hysteresis are of different origin. Furthermore, well-defined and perfectly reproducible hysteresis loops indicates that the structure of the ordered mesoporous materials was not affected during the first intrusion/extrusion cycle, *i.e.*, no fracture or inelastic compression of the materials, even for the sample with the largest pore size/porosity (KIT-6C). This mechanical stability upon hydraulic pressure is remarkable and to the best of our knowledge, this is the first example of successful mercury intrusion/extrusion experiments on KIT-6 silicas. Also, the shape of the mercury intrusion/extrusion hysteresis loops agrees very well with that of the corresponding gas adsorption loop (type H1, Figure 1) indicating the analogy in underlying mechanisms for hysteresis between capillary evaporation/condensation and mercury intrusion/extrusion.[28-31] Figure 2b shows the intrusion curves into KIT-6 silicas (from the first intrusion cycle) as a function of pore diameter over the complete range of probed pores (in semi-logarithmic scale). As explained above, intruded volumes for pores above ca. 10-20 nm are not related to any pores in the KIT-6 materials but rather correspond to interparticle voids between silica particles. Only one very steep increase in the intruded volume is observed for each sample for pores below 10 nm according to the Washburn equation corresponding to the main mesopore size of each KIT-6. It is also important to note that due to technical limitations, *i.e.*, maximum pressure reachable by the instrument is 415000 kPa (60000 psi), no information regarding pores below 4 nm could be obtained with mercury intrusion/extrusion data using the Washburn equation. As a result, in contrast to the situation in KIT-6B and KIT-6C where the system can be completely filled with mercury, a complete filling of the KIT-6A intra-wall pore system is not possible since it would require hydraulic pressures larger than what the porosimetry instrument can generate. From the analysis of the cumulative pore volume

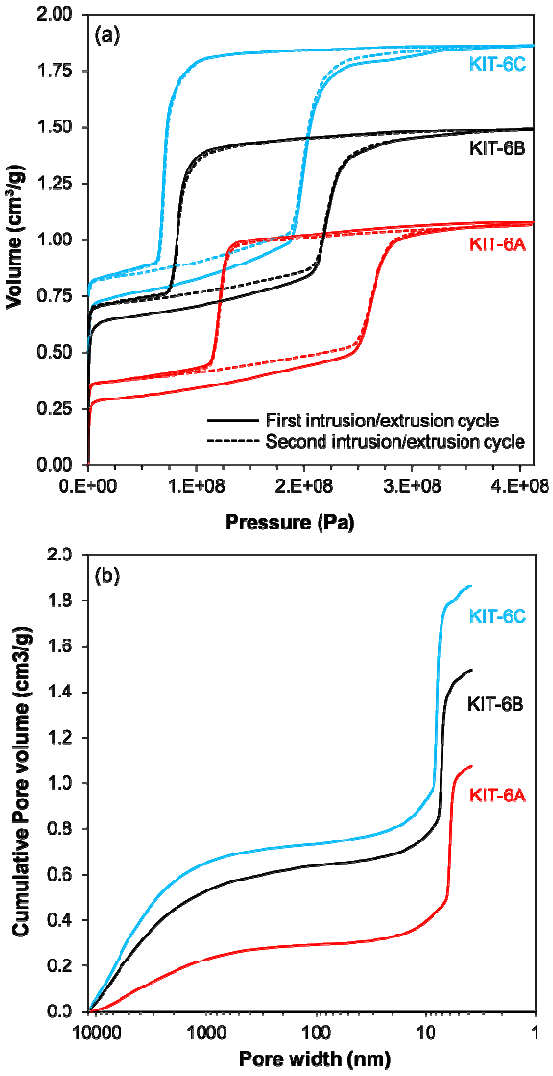

Fig. 2 Mercury intrusion/extrusion curves of two consecutives intrusion/extrusion cycle runs obtained on the same aliquots of KIT-6 samples (a) and corresponding specific pore volume curves obtained for the first mercury intrusion run on each sample over the complete range of probed pores, displayed as a function of pore diameter (b).

curves, specific mesopore volumes of 0.77, 0.83 and 1.11 cm3/g were obtained for KIT-6A, KIT-6B and KIT-6C silicas respectively. Good agreement was found for specific mesopore volumes obtained from gas adsorption (Gurvich and NLDFT) and mercury porosimetry for the KIT-6C silica, but appreciable differences were observed for the KIT-6 silicas with smaller pore size, which is, , as mentioned above, due the inability of mercury porosimetry to probe the intra-wall porosity of these materials.

Figure 3 shows the PSD curves obtained by N_2 physisorption and mercury porosimetry for the KIT-6C sample. The desorption branch of the isotherm was used for pore size analysis because KIT-6 silica material's desorption isotherms are not affected by network effects such as pore blocking or cavitation.[8,62] Indeed perfect H1 type hysteresis loops can be observed for all materials (Figure 1).

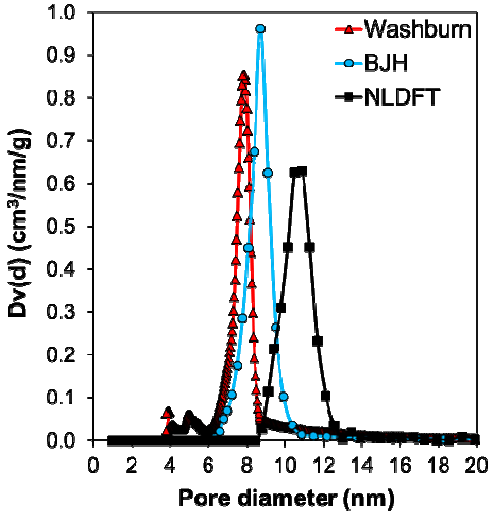

Fig. 3 Pore size analysis of KIT-6C obtained from gas adsorption (using BJH and NLDFT methods applied to the desorption branch) and mercury porosimetry (using Washburn equation and calculated for a contact angle of 145 °).

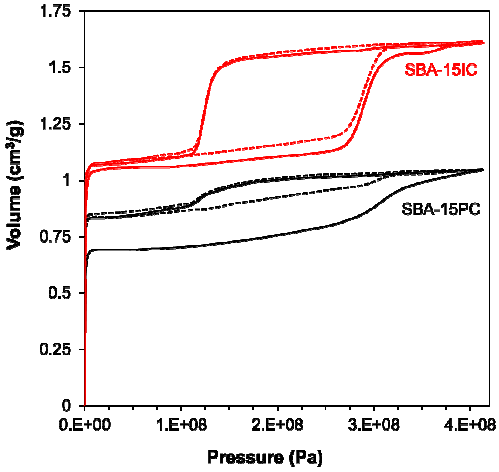

Fig. 4 Mercury intrusion/extrusion curves of two consecutives intrusion/extrusion cycle runs obtained for SBA-15IC and SBA-15PC samples.

Moreover, as discussed above, capillary evaporation (desorption) and mercury intrusion do reflect analogue processes. Hence, as no pore blocking/network effect was found for KIT-6 silicas during desorption, there will be no blocking/network effect which could affect the mercury intrusion behavior. One can thus use the Hg intrusion data to perform a direct comparison of the pore size analysis obtained from mercury porosimetry and gas adsorption. Pore size data from physisorption were obtained by applying both the BJH method which is based on the Kelvin equation,[67] and the NLDFT method. As mentioned in the Introduction, the BJH method and related procedures based on the Kelvin equation can significantly underestimate the pore size for narrow mesopores,[68] while it is known that NLDFT provides accurate pore size information.[8] Indeed, we observed deviations of 20 % for all samples (see Table 1 and Figure S1). In order to calculate the PSD from the Hg intrusion curves, the Washburn equation (which is similar to the Kelvin equation based on the Laplace equation) was applied assuming a contact angle of 145°. As shown in Figure 3, for KIT-6C, (and in table 1) good agreement is found between the pore size obtained from Hg intrusion and the one obtained from the BJH desorption, in line with previous results reported for mesoporous glasses.[29] However both underestimate clearly the KIT-6 silica pore size which is correctly given by the NLDFT method.[62,64] However, it is the first time that it was possible to test the quantitative validity of mercury porosimetry for pore size analysis in more rigorous way by utilizing mesoporous molecular sieves with 3D pore network as reference/model material.

In light of these results, two SBA-15 samples were synthesized and characterized using Hg intrusion/extrusion cycles for comparison purposes. Figure 4 shows Hg intrusion/extrusion data obtained for SBA-15IC and SBA-15PC. One can immediately note that contrarily to KIT-6 materials, SBA-15 ones exhibit two different behaviors upon intrusion/extrusion of mercury. A well-defined and almost perfectly reproducible hysteresis loop is observed between the two runs for SBA-15IC indicating that the porous structure of this particular silica was not noticeably damaged/altered during the successive intrusion/extrusion processes. Such feature also denotes a remarkable mechanical stability upon increasing hydraulic pressures. These results agree well with the ones obtained for 3D KIT6 samples described above. On the other hand, SBA-15PC showed a completely different behaviour. Indeed, the volume of entrapped mercury after the first intrusion/extrusion run is relatively important and the hysteresis between two consecutive intrusion/extrusion cycles is not fully reproducible. Moreover, as compared to SBA-15IC, a lower, less steep and sharp increase in the intruded volume at pressures corresponding to expected pore size for these materials was obtained for SBA-15PC (Figure 4). These major differences are characteristics of a partial collapse of the pore network during the mercury intrusion, i.e., the pore network of SBA-15PC is irreversibly altered/destroyed while mercury fills it. However, it should be noted that the pore structure of SBA-15PC does not totally fractured as some Hg is extruded after the first cycle and is able to be intruded again during the second run meaning that some of the pores remain intact and/or are modified in a way that somehow still allows their accessibility. Such results are of prime importance as they underline two distinct behaviors upon mechanical stability for two materials exhibiting apparently similar porous properties.

Indeed as shown by the nitrogen physisorption isotherms and PSD (at 77.4 K) presented in Figure 5, SBA-15IC and SBA-15PC exhibit the same NLDFT pore size as given by the desorption branch of their respective isotherm. In addition, the two adsorption isotherms exhibit a steep capillary condensation step at high relative pressures characteristic of very high quality samples with narrow distribution of mesopores. Also as point out in Table 1, the two silicas have comparable porosity features. It is therefore necessary to obtain more insights regarding the other properties of these two SBA-15 samples, ultimately seeking to explain why different mechanical stabilities were observed.

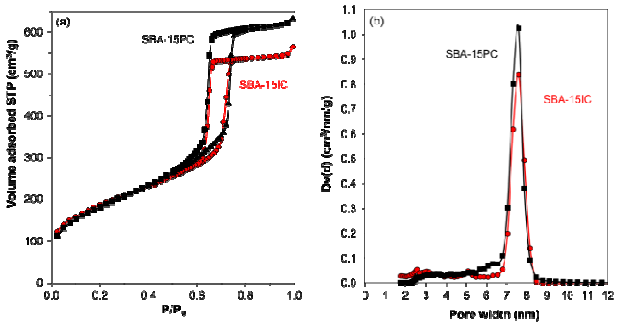

Fig. 5 (a) N_2 (at 77.4 K) adsorption/desorption isotherms and (b) corresponding NLDFT pore size distributions obtained from the desorption branches for SBA-15IC and SBA-15PC.

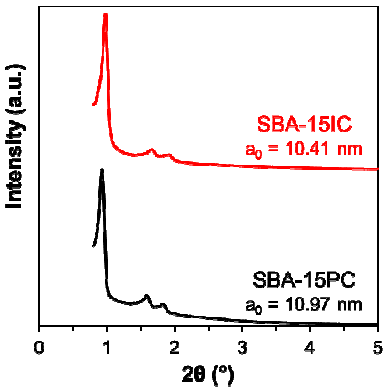

Fig. 6 Low angle powder XRD patterns obtained for SBA-15 silica materials with corresponding lattice cell parameter *a*

Of particular interest are the mesoscopic order and the wall thickness (*t*) of these materials. Indeed, one SBA-15 could exhibit some network distortions and/or thinner walls, rationalizing the differences observed in mercury porosimetry experiments. Figure 6 shows the XRD patterns measured for the calcined SBA-15 samples. All the diffractograms of the template-free materials indicate excellent structural order with the symmetry of the mesophases being commensurate with the hexagonal close packing *P6mm* space group confirming the excellent quality of the materials. The structural parameters obtained from the XRD analyses for the different samples under investigation are also given in Figure 6. Unit cell values of 10.41 nm and 10.97 nm were calculated from XRD data (using the (100) reflection of the 2D hexagonal *p6mm* mesophase) for SBA-15IC and SBA-15PC samples, respectively. The wall thickness of each silica was then obtained by application of a simple relation ($t = a_0 - NLDFT\ pore\ size$). Interestingly, the wall thickness of SBA-15IC (2.81 nm) was found to be lower than the one of SBA-15PC (3.37 nm) demonstrating that collapsing/alteration of SBA-15PC pore network and excellent stability of SBA-15IC during Hg intrusion/extrusion experiments cannot be rationalized by the thickness of their silica walls. XRD patterns and corresponding unit cell values of KIT-6 silicas presented in Figure S2, showed as anticipated, that the acid treatment applied to KIT-6C did not enlarge the unit cell but drastically affected the silica walls, leading to a wall thickness of only about 1 nm (the wall thickness of KIT-6 sample was calculated using the formula: $t = a_0/2 - NLDFT\ pore\ size$). The wall thickness of KIT-6A and KIT-6B was found to be 2.32 and 2.36 nm, respectively. Here also, one can appreciate the remarkable mechanical stability displayed by KIT-6 silicas as these materials underwent several Hg intrusion/extrusion cycles up to 415000 kPa (60000 psi) without showing any collapse of the pore structure (Figure 2) despite having thinner walls compared to SBA-15PC, and even with a wall thickness of only 1 nm in the case of KIT-6C.

Considering these results, it is proposed that the unique behaviour of KIT-6 could rather be related to the known 3D porous network structure of the material.[41,62] Based on our results, SBA15IC seems to behave similar to KIT-6 silicas with regard to mechanical stability, and this could indicate, in line with previous work on the topic including our,[43,46,62] that this particular SBA-15 indeed consist of a 3D-like system where main mesopores are connected together via relatively large mesoporous interconnections. On the contrary, SBA15PC demonstrates much weaker mechanical stability, i.e., the mercury intrusion/extrusion results are in line with similar results reported in the literature.[34-37] SBA15PC silica was synthesized at 30°C (i.e., 5 °C lower than SBA-15IC), using 33% more TEOS and hydrothermally treated at higher temperature as compared to SBA-15IC. Although it is commonly expected that SBA-15s hydrothermally treated at higher temperatures (especially above 100°C) will always result in a material exhibiting a 3D-like porous network, one has to remember that it is true only if all other synthesis parameters are kept constant. Indeed as reported recently,[43] one may finely and effectively tune the porous structure of SBA-15 materials by synergistically modifying different synthesis parameters simultaneously. As a result, the aging temperature, even though being important, is not the only decisive parameter influencing the final porosity of the silicas.

Hence, the conditions used to obtain SBA-15PC, as confirmed by vast majority of published data on SBA-15 preparation[39-49,69,70] and by SAXRD data discussed above, led to a material with a noticeably larger wall thickness. Therefore, one cannot rule out that such synthesis conditions would then also lead to a different pore network topology, i.e., instead of a highly interconnected mesopore system, SBA-15PC would rather exhibit a porous topology that could be viewed as an arrangement of cylindrical mesopores, only connected through micropores or narrow mesopores. Such possible differences in pore network topology could ultimately affect mechanical stability. However, despite a solid body of evidence connecting sorption behaviour and pore topology of ordered mesoporous silicas,[43,62] further confirmation from independent advanced imaging or nanocasting techniques would be required to fully elucidate the pore network differences between these two SBA-15 materials and their correlation with mechanical stability; yet the latter being beyond the scope of the present work.

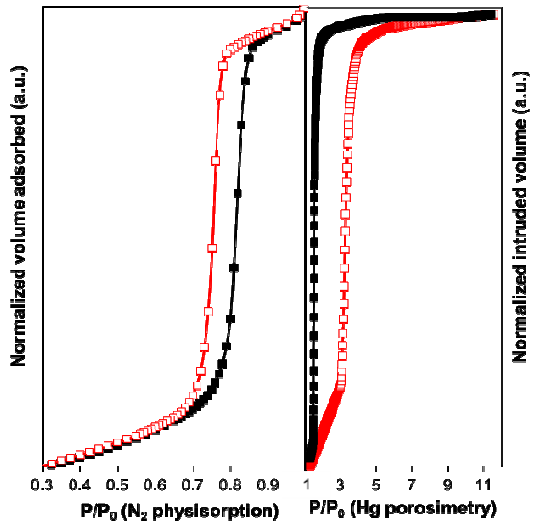

Fig. 7 Adsorption (solid) and desorption (hollow) isotherm of a wetting fluid (N2 at 77 K, normalized to the total adsorption capacity, left) obtained for KIT-6C and corresponding equivalent gas sorption isotherm of a non-wetting fluid (Hg at 298 K, normalized to the total amount intruded, right part) converted from the mercury porosimetry data using Lowell and Shields equation.

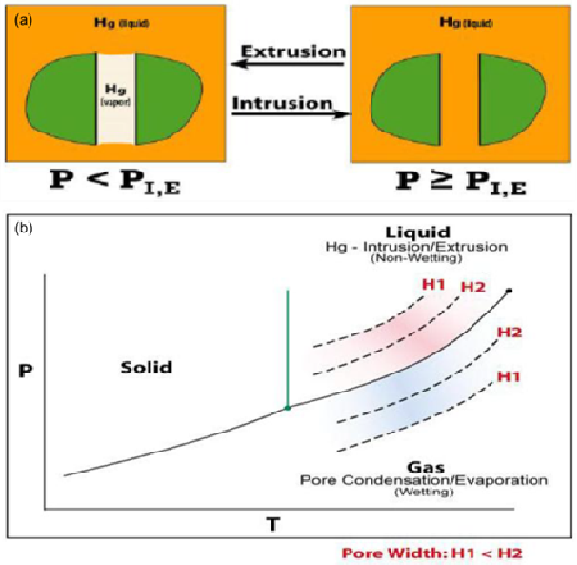

Fig.8 Schematized representation of the mercury intrusion/extrusion process into a single pores ($P_{I,E}$ is the hydraulic pressure where intrusion/extrusion occurs) (a) and schematic diagram depicting the symmetry between pore condensation/evaporation and Hg intrusion/extrusion, which represents the phase behavior of wetting and non-wetting fluids, respectively (please note that in this schematics we do not illustrate pore critical points, i.e., we focus here only the subcritical region of the confined pore fluid) (b).

Equivalency of mercury porosimetry and gas sorption: Phase behaviour of wetting and non-wetting fluids in mesopores

As discussed above, capillary condensation/evaporation occurring into the pores during physisorption experiments and mercury intrusion/extrusion can be seen as thermodynamically equivalent processes. This had already been discussed in the early 80's and 90's based on macroscopic thermodynamic approaches[23,71] and recently by applying methods based on statistical mechanics such as mean field density functional theory and methods based on molecular simulation.[28-30] Within this context, Lowell and Shields have proposed an expression that relates the hydraulic pressure to the pressure of the mercury vapor that coexists with the liquid mercury inside the porous material:[9,23]

$$\frac{P_v'}{P_0} = \exp\left(\frac{P_h V_l}{RT}\right)$$

Where P_v' is the mercury vapor pressure, P_0 is the saturation pressure, P_h is the hydraulic pressure and V_l is the molar volume of the bulk liquid.

More details regarding the derivation of this equation can be found elsewhere.[28] Hence, with this, it became possible to transform the hydraulic pressure scale of an intrusion experiment into a Hg vapor pressure, i.e. converting mercury intrusion/extrusion data into mercury adsorption/desorption isotherms. While Lowell and Shields had used this approach equation to convert mercury intrusion/extrusion data obtained on a variety of porous materials into mercury adsorption/desorption isotherms, all this materials exhibited highly complex and disordered pore networks.[9,23] Here we utilize for the first time highly ordered mesoporous molecular sieves such as KIT-6 silica for investigating the analogies between condensation-evaporation mechanisms of a wetting fluid (N_2 at 77 K) and of a non-wetting fluid (Hg at room temperature), which allowed us to investigate these phenomena also as a function of pore size. Results for KIT-6C are presented in Figure 7. One can note the striking reversed symmetry observed between the two sets of curves. While capillary condensation of N_2, occurs at pressures smaller than the saturation pressures, the vapor-liquid phase transition for mercury occurs at pressures which are larger than the saturation pressure. This finding is perfectly in line with early work from Lowell and Shields,[9,23] as well as recent theoretical calculations and experimental results reported by Monson and Thommes *et al.* for porous glass samples.[28-30] However, utilizing mesoporous molecular sieves of known pore geometry and size allows us here, as mentioned above, to quantitatively check the effect of pore size on the pore evaporation/condensation pressure of mercury in cylindrical silica pores, i.e., nitrogen and mercury adsorption/desorption isotherms and corresponding mercury vapour isotherms for KIT-A and KIT-6B silicas are presented in Figure S3. It is clearly shown that the relative pressure P/P_0 where pore condensation occurs for the non-wetting fluid (mercury) increases with decreasing pore diameter, while for a wetting fluid such as nitrogen the opposite trend is observed.

These experiments clearly confirm the thermodynamic equivalency of underlying mechanisms for capillary

evaporation/condensation of a wetting fluid and Hg intrusion/extrusion. Hence, our results (Figures 7 and S3) allow one to suggest the schematic representation of the phase behaviour of a wetting fluid (gas adsorption) and the non-wetting fluid mercury in mesopores (Figure 8).

Conclusions

We have performed a systematic study of nitrogen adsorption at 77 K and mercury porosimetry experiments on high quality 3D KIT-6 ordered mesoporous silicas with pore diameters in the 8-11 nm range. Remarkably, no collapse of the pore structure was observed when Hg intrusion/extrusion cycles were performed up to pressures of ca. 415000 kPa (60 000 psi) even for highly porous materials with pore diameters up to 11 nm and exhibiting a wall thickness of only 1 nm. To the best of our knowledge, this is the first successful example of Hg porosimetry on KIT-6 silica materials. Hence it was possible to utilize KIT-6 mesoporous molecular sieves of known pore sizes for quantitatively testing the validity of the Washburn equation (mercury porosimetry) for pore size analysis. The results clearly demonstrate that similar to the Kelvin equation-based approaches used in physisorption (e.g. BJH) the pore size derived from mercury porosimetry significantly underestimates the real pore size for narrow mesopores. KIT-6 silicas also allowed for investigating the analogies between condensation-evaporation mechanisms of wetting (here N_2 at 77 K) and non-wetting fluid (Hg at room temperature) as a function of pore size. These data confirm the thermodynamic consistency between mercury intrusion/extrusion and capillary evaporation/condensation. Contrary to KIT-6 silicas, Hg porosimetry experiments on SBA-15 materials of identical pore diameter exhibited inconsistent behavior in a sense that both reversible Hg intrusion/extrusion data and partial collapse of the pore structure were observed.

Summarizing, our work clearly demonstrates that combining advanced physical adsorption and Hg porosimetry studies provide a more thorough understanding of textural features and shed some light into fundamental questions concerning the effect of confinement on the phase behavior of wetting and non-wetting fluids. Further work is however needed in order to unambiguously elucidate and complement the nature and relationship between pore network characteristics (including dimensionality) and mechanical stability.

Acknowledgements

Prof. R. Ryoo and his co-workers (KAIST, Daejeon, Republic of Korea) are acknowledged for low-angle-XRD measurements. F.K. acknowledges support from the Natural Sciences and Research Council of Canada (NSERC)

Notes and references

[1] (a) J. Rouquerol, G. V. Baron, R. Denoyel, H. Giesche, J. Groen, P. Klobes, P. Levitz, A. V. Neimark, S. Rigby, R. Skudas, K. S. W. Sing, M. Thommes, K. K. Unger, *Pure Appl. Chem.*, 2012, **1**, 107; (b) J. Rouquerol, G. V. Baron, R. Denoyel, H. Giesche, J. Groen, P. Klobes, P. Levitz, A. V. Neimark, S. Rigby, R. Skudas, K. S. W. Sing, M. Thommes, K. K. Unger, *Micro. Meso. Mater.*, 2012, **154**, 6.
[2] Y. Sakamoto, M. Kaneda, O. Terasaki, D. Y. Zhao, J. M. Kim, G. D. Stucky, H. J. Shim, R. Ryoo, *Nature*, 2000, **408**, 449.
[3] M. Thommes, *Chem. Ing. Technik*, 2010, **82**, 1059.
[4] M. Thommes, K. A. Cychosz, *Adsorption*, 2014, **20**, 233.
[5] M. Thommes, *Stud. Surf. Sci. Catal.*, 2007, **168**, 495.
[6] M. Thommes in Nanoporous Materials, Science & Engineering, G. Q. Lu, X. S. Zhao (Editors), 2004, Chapter **11**, Imperial College Press.
[7] J. Landers, G. Y. Gor, A. V. Neimark, *Colloids Surf. A*, 2013, **437**, 3.
[8] M. Thommes, K. Kaneko, A. V. Neimark, J. P. Olivier, F. Rodriguez-Reinoso, J. Rouquerol, K. S. W. Sing, *Pure Appl. Chem.*, 2015, **87**, 1051.
[9] S. Lowell, J. Shields, M. A. Thomas, M. Thommes, Characterization of Porous Solids and Powders: Surface Area, Pore Size and Density, 2004, Springer, The Netherlands.
[10] C. León y León, *Adv. Colloid Interface Sci.*, 1998, **76**, 341.
[11] E. W. Washburn, *Proc. Nat. Acad. Sci. USA*, 1921, **7**, 115.
[12] J. C. Groen, L. A. A. Pfeffer, J. Perez-Ramirez, *Stud. Surf. Sci. Catal.*, 2002, **144**, 91.
[13] L. M. Pismen, *Doklady Akademii Nauk SSSR*, 1973, **211**, 1398.
[14] A. V. Neimark, *Colloid J. of the USSR*, 1984, **46**, 639.
[15] C. D. Tsakiroglou, A. C. Payatakes, *Adv. Colloid Interf. Sci.*, 1998, **75**, 215.
[16] A.V. Neimark, *Colloid J. of the USSR*, 1985, **47**, 67;
[17] L. Moscou, S. Lub, *Powder Tech.*, 1981, **29**, 45.
[18] S. Rigby, *Stud. Surf. Sci. Catal.*, 2002, **144**, 185.
[19] S. P. Rigby, I. O. Evbuoumwan, M. J. Watt-Smith, K. Edler, R. S. Fletcher, *Part. Part. Syst. Charact.*, 2006, **82**.
[20] C. Felipe, F. Rojas, I. Kornhauser, M. Thommes, G. Zgrablich, *Ads. Sci. Technol.*, 2006, **8**, 623.
[21] H. Giesche, *Part. Part. Syst. Charact.,* 2006, **23**, 9.
[22] H. Giesche, *Mat. Res. Soc. Symp. Proc.,* 1996, **431**, 151.
[23] (a) S. Lowell, J. E. Shields, *J. Colloid. Interface Sci.*, 1981, **80**, 192; (b) S. Lowell, J. E. Shields, *J. Colloid. Interface Sci.,* 1981, **83**, 273.
[24] G. Salmas, G. J. Androutsopolous, *J. Colloid Interface Sci.*, 2001, **239**, 178.
[25] M. Day, I. B. Parker, J. bell, M. Thomas, R. Fltecher, J. Duffie in: Characterization of Porous Solids II, J. Rouquerol, F. Rodriguez-Reinoso, K. S. W. Sing, K. K. Unger (Eds.), Amsterdam, 1991, p. 75

[26] M. Day, I. B. Parker, J. Bell, R. Fletcher, J. Duffe, K. S. W. Sing, D. Nicholson, *Stud. Surf. Sci. Catal.*, 1994, **87**, 225.
[27] G. Zgrablich, S. Mendioroz, L. Daza, J. Pajares, V. Mayagotia, F. Rojas, W. C. Conner, *Langmuir*, 1991, **7**, 779.
[28] F. Porcheron, P. A. Monson, M. Thommes, *Langmuir*, 2004, **20**, 6482.
[29] F. Porcheron, M. Thommes, R. Ahmad, P. A. Monson, *Langmuir*, 2007, **23**, 3372.
[30] F. Porcheron, P. A. Monson, *Langmuir*, 2005, **21**, 3179.
[31] M. Thommes, R. Skudas, K. K. Unger, D. Lubda, *J. Chromato. A*, 2008, **1191**, 57.
[32] S. P. Rigby, R. S. Fletcher, S. N. Riley, *Chem. Eng. Sci.*, 2004, **59**, 41.
[33] N. Andersson, P. C. A. Alberius, J. S. Pedersen, L. Bergstrom, *Micro. Meso. Mater.*, 2004, **72**, 175.
[34] A. Vinu, M. Hartmann, *Langmuir*, 2002, **18**, 8010.
[35] A. Vinu, V. Murugesan, W. Bohlmann, M. Hartmann, *J. Phys. Chem. B*, 2004, **108**, 11496.
[36] A. Galarneau, B. Lefèvre, H. Cambon, B. Coasne, S. Valange, Z. Gabelica, J.-P. Bellat, F. Di Renzo, *J Phys. Chem. C*, 2008, **112**, 12921.
[37] B. Coasne, A. Galarneau, F. Di Renzo, R. J. M. Pellenq, R. J. M., *J. Phys. Chem. C*, 2009, **113**, 1953.
[38] D. Y. Zhao, Q. S. Huo, J. L. Feng, B. F. Chmelka, G. D. Stucky, *J. Am. Chem. Soc.*, 1998, **120**, 6024.
[39] F. Kleitz, S. H. Choi, R. Ryoo, *Chem. Commun.*, 2003, **2136**.
[40] J. S. Beck, J. C. Vartuli, W. J. Roth, M. E. Leonowicz, C. T. Kresge, K. D. Schmitt, C. T.-W. Chu, D. H. Olson, E. W. Sheppard, S. B. McCullen, J. B. Higgins, J. L. Schenkler, *J. Am. Chem. Soc.*, 1992, **114**, 10834.
[41] T.-W. Kim, F. Kleitz, B. Paul, R. Ryoo, *J. Am. Chem. Soc.*, 2005, **127**, 7601.
[42] V. Alfredsson, M. W. Andersson, *Chem. Mater.*, 1996, **8**, 1141.
[43] R. Guillet-Nicolas, F. Bérubé, T.-W. Kim, M. Thommes, F. Kleitz, *Stud. Surf. Sci. Catal.*, 2008, **174**, 141.
[44] M. Kruk, M. Jaroniec, C. H. Ko, R. Ryoo, *Chem. Mater.*, 2000, **12**, 1961.
[45] R. Ryoo, C. H. Ko, M. Kruk, V. Antochshuk, M. Jaroniec, *J. Phys. Chem. B*, 2000, **104**, 11465.
[46] A. Galarneau, N. Cambon, F. Di Renzo, R. Ryoo, M. Choi, F. Fajula, *New J. Chem.*, 2003, **27**, 73.
[47] Y. Sakamoto, T.-W. Kim, R. Ryoo, O. Terasaki, *Angew. Chem. Int. Ed.*, 2004, **43**, 5231.
[48] T.-W. Kim, L. A. Solovyov, J. Mater. Chem., 2006, **16**, 1445.
[49] A. Rumplecker, F. Kleitz, E. L. Salabas, F. Schüth, *Chem. Mater.*, 2007, **19**, 485.
[50] H. Tuysuz, F. Schüth, *Adv. Catal.*, 2012, **55**, 127.
[51] A. Taguchi, F. Schüth, *Micro. Meso. Mater.*, 2006, **77**, 1.
[52] Z. Wu, D. Y. Zhao, *Chem. Commun.*, 2011, **47**, 3332.
[53] N. Calin, A. Galarneau, T. Cacciaguerra, R. Denoyel, F. Fajula, *C. R. Chimie*, 2010, **13**, 199.
[54] T.-W. Kim, I. I. Slowing, P.-W. Chung, V. S.-Y. Lin, *ACS Nano*, 2011, **5**, 360.
[55] A.-H. Lu, F. Schüth, *Adv. Mater.*, 2006, **18**, 1793.
[56] Y. Ren, Z. Ma, P. G. Bruce, *Chem. Soc. Rev.*, 2012, **41**, 4909.
[57] Y. Shi, Y. Wan, D. Y. Zhao., *Chem. Soc. Rev.*, 2011, **40**, 3854.
[58] C.-M. Yang, B. Zibrowius, W. Schmidt, F. Schüth, *Chem. Mater.*, 2004, **16**, 2918.
[59] M. Choi, W. Heo, F. Kleitz, R. Ryoo, *Chem. Commun.*, 2003, 1340.
[60] J. Simon, S. Saffer, C. J. Kim, *J. Microelectromech. Syst.*, 1997, **6**, 208.
[61] ISO 15901-1 "Pore size distribution and porosity of solid materials by mercury porosimetry and gas adsorption – Part 2: Analysis of macropores by mercury porosimetry".
[62] F. Kleitz, F. Bérubé, R. Guillet-Nicolas, C.-M. Yang, M. Thommes, *J. Phys. Chem. C*, 2010, **114**, 9344.
[63] P. I. Ravikovitch, A. V. Neimark, *Langmuir*, 2000, **16**, 2419.
[64] K. Schumacher, P. I. Ravikovitch, A. Du Chesne, A. V. Neimark, K. K. Unger, *Langmuir*, 2000, **16**, 4648.
[65] A. V. Neimark, P. I. Ravikovitch, A. Vishnyakov, *J. Phys. Condens. Matter.*, 2003, **15**, 347.
[66] A. V. Neimark, P. I. Ravikovitch, *Micro. Meso. Mater.*, 2001, **44**, 697.
[67] E. P. Barrett, L. G. Joyner, P. H. Halenda, *J. Am. Chem. Soc.*, 1951, **73**, 373.
[68] M. Thommes, Physical Adsorption Characterization of Ordered and Amorphous Mesoporous Materials, in Nanoporous Materials: Science and Engineering (Eds: G. Q. Lu, X. S. Zhao), Imperial College Press, Oxford, **317**, 2004.
[69] a) V. Alfredsson, H. Wennerström, *Acc. Chem. Res.*, 2015, **48**, 1891; b) T. Kjellman, S. Asahina, J. Schmitt, M. Impéror-Clerc, O. Terasaki, V. Alfredsson, *Chem. Mater.*, 2013, **25**, 4105
[70] a) V. Zholobenko, A. Y. Khodakov, M. Impéror-Clerc, D. Durand, I. Grillo, *Adv Colloid Interface Sci.*, 2008, **142**, 67; b) S. Manet, A. Lecchi, M. Impéror-Clerc, V. Zholobenko‡, D. Durand, C. L. P. Oliveira, J. S. Pedersen, I. Grillo, F. Meneau, C. Rochas, *J. Phys. Chem. B*, 2011, **115**, 11318.
[71] K. L. Murray, N. A. Seaton, M. A. Day, *Langmuir*, 1999, **15**, 8155.

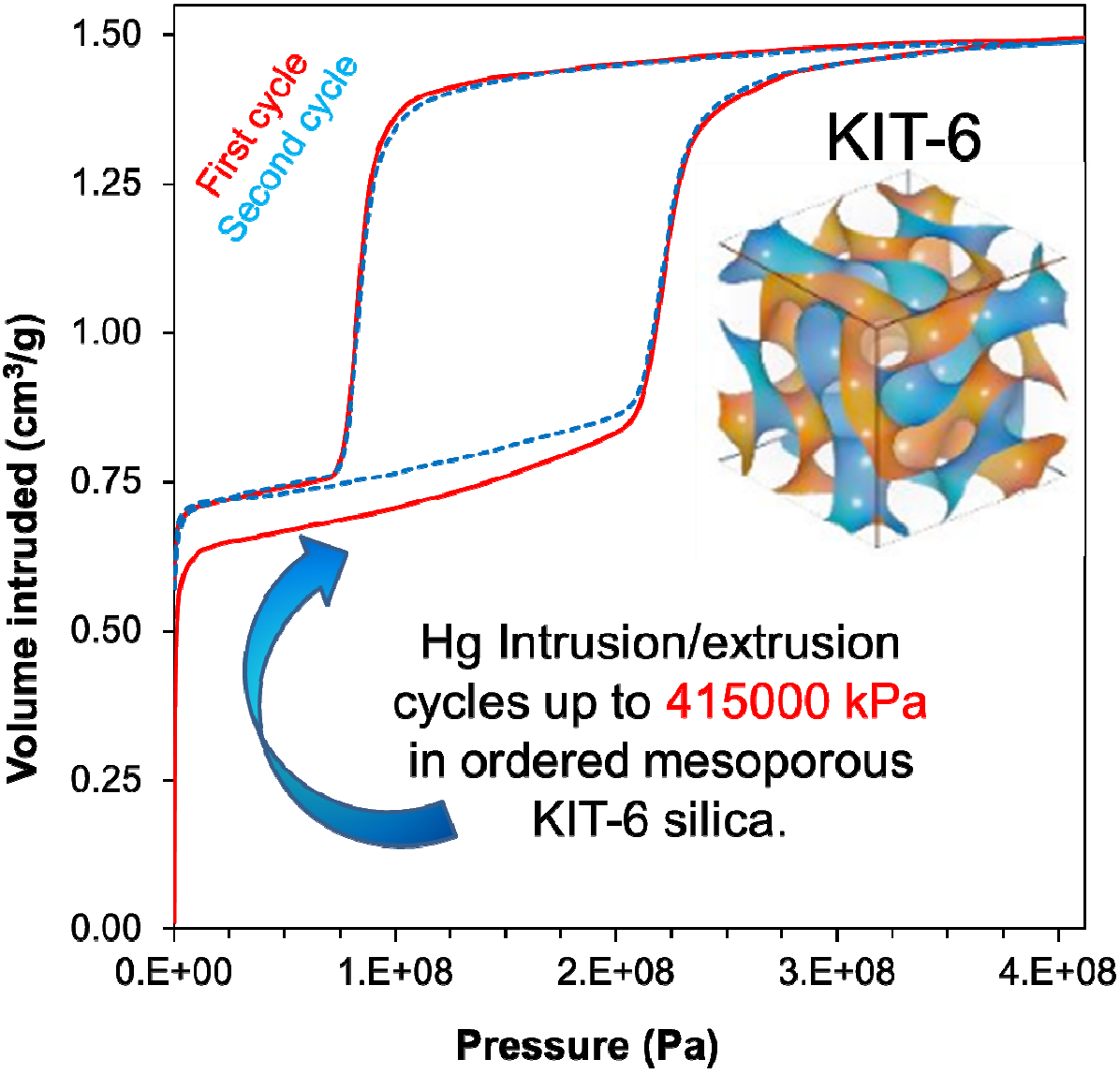

First successful example of Hg porosimetry on KIT-6 silica is demonstrated. . This study provides a more thorough understanding of the textural properties of both mesostructures particularly in terms of pore interconnectivity and network effects.